

Article

Exploring Synergies: Tailoring Electrical Conductivity in Novel Corn Starch and Natural Rubber Polymer Composites through Varied Carbon Additives

Miftahul Fiqri¹, Syahrul Humaidi^{1*}, Erna Frida¹, Estananto²

Article Info

Article history :

Received February 23, 2024
Revised May 15, 2024
Accepted May 23, 2024
Published June 30, 2024

Keywords :

Conductive polymer composites, carbon additives, crosslinking method, electrical conductivity

¹Postgraduate Programme in Physics, Faculty of Mathematics and Science, Universitas Sumatera Utara, Medan, Indonesia

²Advanced Functional Materials Research Group, Faculty of Industrial Technology, Institut Teknologi Bandung, Bandung, Indonesia

Abstract. Conductive polymer composites were synthesized using a crosslinking method, enhancing conductivity through the incorporation of carbon additives. Non-conductive natural polymers, corn starch, and natural rubber were blended with carboxymethyl cellulose (CMC) as a crosslinking agent, enhancing polymer bonding. CMC also served as a compatibilizer, improving corn starch properties. Glycerol acted as a plasticizer, enhancing flexibility and processability. Addition of carbon nanotube (CNT), graphite, and carbon foam yielded low-density materials, with carbon foam providing optimal porosity. The crystalline properties mirrored the added conductive carbon, while the chemical structure remained unchanged. At 0.1 Hz, electrical conductivity varied: 1.192×10^{-7} S.cm⁻¹ (no carbon), 6.123×10^{-4} S.cm⁻¹ (CNT), 7.656×10^{-4} S.cm⁻¹ (graphite), and 3.134×10^{-2} S.cm⁻¹ (carbon foam). Graphite incorporation demonstrated an electrical conductivity of 7.838×10^{-4} S.cm⁻¹. The introduced carbon additives facilitated a conductive pathway in corn starch-based polymer composites, elevating material conductivity.

This is an open access article under the [CC-BY](https://creativecommons.org/licenses/by/4.0/) license.



This is an open access article distributed under the Creative Commons 4.0 Attribution License, which permits unrestricted use, distribution, and reproduction in any medium, provided the original work is properly cited. ©2024 by author.

Corresponding Author :

Syahrul Humaidi
Postgraduate Programme in Physics, Faculty of Mathematics and Science,
Universitas Sumatera Utara, Medan, Indonesia
Email: syahrul1@usu.ac.id

1. Introduction

In recent decades, the exploration of conductive polymer composite materials has emerged as a pivotal area of research globally, driven by their remarkable mechanical and electrical properties, poised for applications across polymer science [1], electronic technology [2], defense sectors [3], and medical innovations [4]. These materials offer unprecedented versatility, enabling advancements in flexible electronics [5], lightweight structural components [6], electromagnetic shielding [7], and biocompatible implants [8]. Moreover, their tunable conductivity, coupled with inherent polymer flexibility and processability, opens avenues for innovative designs in wearable devices, smart textiles, energy storage systems, and biosensors, revolutionizing diverse industries and enhancing quality of life [9-10].

Generally, polymers exhibit low electrical conductivity or act as insulators. However, through various studies, it has been discovered that certain polymer materials can acquire conductive properties by adding specific substances, resulting in the formation of a conductive second phase [10-11]. Conductive polymers are a highly sought-after novel material among researchers due to their unique electrical and magnetic properties, as well as the ease of synthesis. In semiconductor physics, the addition of certain substances causing defects in semiconductors (doping process) leads to the formation of extrinsic semiconductor materials. In contrast, intrinsic conductive polymer materials explain the conductive properties in the form of doping. This differs from extrinsic conductive polymers [12], where conductivity is achieved by blending non-conductive polymers with conductive materials such as metals or carbon powders to form composites [13].

Conductive polymers have numerous potential applications today, with their properties depending on the conductive reinforcement material, matrix, and manufacturing processes, which ultimately determine their characteristics. The 1977 publication by Shirakawa and colleagues marked the beginning of global interest in the study of conductive polymers. This research highlighted changes in the electrical properties of polyethylene before and after doping. They found that oxidation with chlorine, bromine, or iodine vapor could increase the conductivity of polyacetylene layers by more than 10^9 times compared to control layers [14].

The treatment involving the addition of conductive materials is referred to as "doping," drawing an analogy to the doping process used in semiconductors. Other oxidizing doping agents have been employed, including arsenic pentafluoride, and reducing agents such as sodium metal have also been used. Chemical doping like this transforms polyacetylene from an insulator or semiconductor into a conductor [15]. Currently, research on conductive polymer composites has gained momentum due to various advantages [16], such as the combination of metallic and plastic properties [17], making them durable over time [18], possessing high conductivity [11], and being light-transmissive or transparent [19]. Additionally, the production process is easy, cost-effective, and efficient.

In the past five years, organic or biopolymer-based polysaccharide polymers such as starch, with the addition of other additives, have garnered significant attention in polymer research due to their ease of synthesis and superior mechanical characteristics. Chatterjee and colleagues (2023) noted that starch-based biopolymers exhibit good mechanical properties suitable for medical applications [20]. These superior characteristics can be widely used as raw materials in the engineering of human body tissues, bone barrier membranes, skin, and even applied as delivery systems in the medical treatment process.

The synthesis of corn starch-based biopolymers with the addition of a liquid natural rubber and optimal mechanical characteristics, supported by a carboxymethyl cellulose (CMC) crosslinking agent, successfully enhanced intermolecular polymer bonding and supported the interfacial phase bonding process [21]. Kwon and colleagues' publication (2021) on carbon-based polymer composites summarized various conductivity characteristics based on carbon fillers such as graphite, carbon nanotubes (CNT), and carbon foam, enhancing the conductivity properties of polymer composite

materials [22]. The absence of research related to conductive polymer composites from natural polymer materials like corn starch adds a unique appeal to initiating studies on this topic. Fabricating these materials can undoubtedly enhance their advantages, expanding their applications across various technological fields [23].

The ease of fabricating corn starch and natural rubber-based polymer composites with carbon dopants is undoubtedly one of the reasons why research on this topic is worthwhile. Additionally, carbon materials can provide conductivity stimulus to natural polymer composite materials made from corn starch, making them applicable in the field of electricity, such as batteries, solar cells, or fuel cells [5]. Building on the aforementioned background, this research will focus on the synthesis and characterization of polysaccharide-based polymer composites derived from corn starch and natural rubber, with the addition of carbon additives, to obtain conductive polymer composite materials.

2. Experimental Section

2.1. Samples Preparation

The total mass of the prepared polymer composite samples is standardized at 10 grams per sample. The synthesis process begins with the incorporation of three primary precursors: 1 gram of natural rubber, a blend of 70% corn starch and 30% glycerol totaling 9 grams, referred to as PJG, which is stirred in a water bath at 80°C for 30 minutes at 125 rpm. To facilitate the crosslinking method, a mixture of 1.8 grams of CMC and 18 ml of distilled water is prepared as the third precursor and stirred for 30 minutes at 100 rpm without heat treatment. Subsequently, the three precursors are combined in a chemical glass container and stirred for 1 hour at a speed of 250 rpm without heat treatment. The addition of CNT, graphite, and carbon foam powders follows, each constituting 6% of the total composite mass or 0.6 grams, resulting in three distinct sample types: CGG-C, CGG-G, and CGG-F, respectively. Samples devoid of conductive carbon additions are denoted as CGG. Finally, each sample undergoes drying in an oven at 60°C for 24 hours.

The addition of each conductive carbon, 6% of the total polymer matrix, is adjusted based on the 2022 publication by Xu, stating that the optimum composition achievable for conductive carbon in the polymer matrix is 6% of its total mass. Deviating from this amount may reduce the achievable optimum conductivity if less, while exceeding it may potentially diminish mechanical capabilities and lead to structural defects in the polymer crystal [13].

Table 1. Sample's Design and Composition

No.	PJG (gr)	Natural rubber (gr)	CMC (gr)	Conductive carbon (gr)	Sample's code
1				-	CGG
2	9	1	1.8	0.6 CNT	CGG-C
3				0.6 Graphite	CGG-G
4				0.6 Carbon foam	CGG-F

2.2. Characterization

The prepared samples undergo a series of tests, starting with density testing, surface morphology characterization using SEM, and crystalline property characterization through XRD analysis with the assistance of the Match! application. Chemical structure identification of the samples is carried out through FTIR analysis. Electrical conductivity testing is performed as a function of frequency after mixing the samples with 1-2 ml of ethylene glycol to form a thick paste [24]. Subsequently, the prepared and sterilized electrodes are coated with the adhesive solution using the doctor blading coating technique. Afterward, the coated electrodes are heated at 75°C for 1 hour in an oven and allowed to cool to room temperature, making the samples ready for conductivity testing.

3. Results and Discussion

3.1. Fourier Transform Infra-Red (FTIR)

Figure 1 displays the FTIR spectra of corn starch, natural rubber, and CGG samples. It can be observed that the FTIR spectrum of corn starch exhibits four main peaks. At the wavenumber of 1416.38 cm^{-1} , the strongest peak with an absorbance of 10.84% indicates the presence of the -OH (hydroxyl) bonding group. The second peak, which is the weakest, appears at the wavenumber of 2176.76 cm^{-1} with an absorbance of 4.89%, signifying the stretching of C-H bonds. The next peak is observed at the wavenumber of 2363.13 cm^{-1} with an absorbance of 5.48%, also indicating C-H stretching. The last peak, characterized by a relatively sharp slope and indicative of OH (hydroxyl) stretching, is located at the wavenumber of 3063.87 cm^{-1} with an absorbance of 8.37%. The distribution of molecular bonding peaks in corn starch aligns with previous research findings.

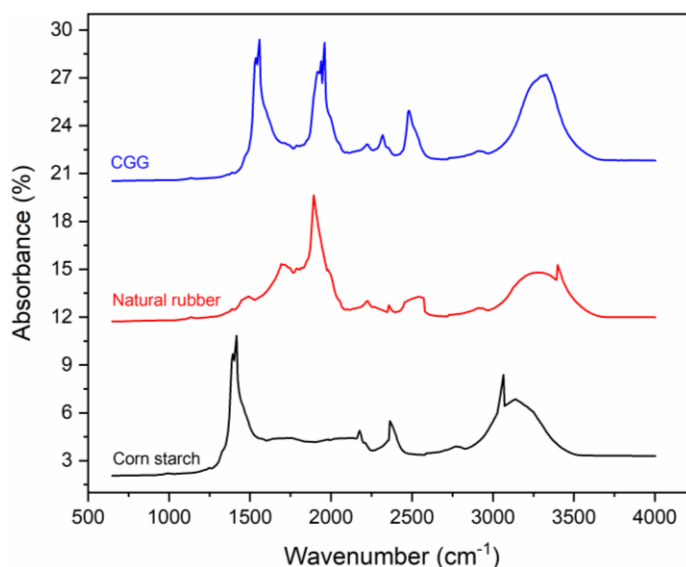


Figure 1. FTIR spectra of corn starch, natural rubber and CGG samples

In contrast to the FTIR spectrum of corn starch with four main peaks, natural rubber exhibits a spectrum pattern with five main peaks spread across the wavenumber range of $1500 - 3500\text{ cm}^{-1}$. The highest peak is located at the wavenumber of 1893.48 cm^{-1} with an absorbance of 10.99%, indicating the stretching of alkene functional groups (C=C). The peak with significant absorbance at the wavenumber of 3399.33 cm^{-1} indicates C-H bonding with an intensity of 6.63%. Other absorbance peaks show characteristics of double-bonded C-H stretching with C=C. The FTIR spectrum of the CGG sample reveals six main absorbance peaks, with four of them having relatively high absorbance levels. The absorbance peak at the wavenumber of 1558.02 cm^{-1} indicates the presence of -OH bonding groups from molecular bonds in corn starch, showing a peak shift to the right by 141.64 cm^{-1} . The absorbance peak at the wavenumber of 1960.58 cm^{-1} indicates stretching of alkene functional groups (C=C) from molecular bonds in natural rubber [25].

Other absorbance peaks in the wavenumber range of $2500 - 3500\text{ cm}^{-1}$ are also a combination of absorbance peaks from corn starch and natural rubber. This indicates that the mixing of the two polymers successfully forms a polymer composite with absorbance peaks in molecular bonds that are distributed according to the characteristics of each component. Additionally, in broad terms, there is no formation of new absorbance peaks in the FTIR spectrum of the CGG sample that do not originate from its two main constituent materials, namely corn starch and natural rubber.

Figure 2 shows the comparison between the FTIR spectra of CGG, CGG-C, CGG-G, and CGG-F samples. It can be observed that the addition of 0.6 grams of CNT does not lead to the formation of a new composite. The FTIR spectrum of CGG-C has six main peaks identical to the CGG sample. An absorbance peak is detected at the wavenumber of 1543.11 cm^{-1} with an intensity of 20.34%, indicating the -OH bonding group. Similarly, the addition of 0.6 grams of graphite does not result in the formation of a new composite. The FTIR spectrum of CGG-G also has six main peaks identical to the CGG sample, with the absorbance peak detected at the same wavenumber as CGG-C, namely 1543.11 cm^{-1} , but with a reduced intensity of 19.84%, indicating the -OH bonding group. The decreased intensity of absorbance suggests a reduction in the quantity (per unit volume) of -OH bonding functional groups, implying molecular bonds have contracted, and molecular bonds in the -OH bonding groups formed have weakened [26]. The intensity weakening in other peaks is also caused by graphite's strong anti-aggregation (separation) morphology, influencing the molecular bonds formed during the interaction with the CGG polymer composite [27]. The addition of 0.6 grams of carbon foam to CGG also does not alter the structure of the formed molecules, as evidenced by the identical FTIR spectrum of CGG-F to the CGG sample, despite a decrease in absorbance intensity in some spectrum peaks.

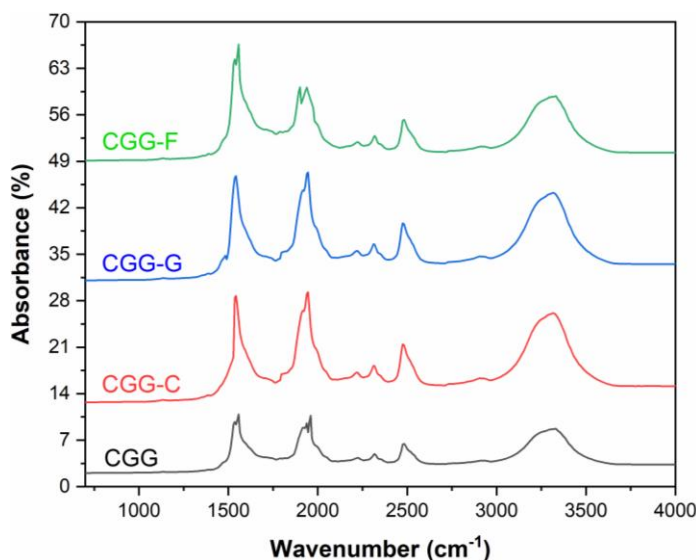


Figure 2. FTIR spectra of CGG, CGG-C, CGG-G, and CGG-F samples

3.2. Density and Porosity

The density of the polymer composite is measured to analyze the influence of different conductive carbon compositions on the empty spaces within the material. Similar to density, porosity is also an indicator of the quantity of empty space (pores) within the conductive polymer composite material. Porosity (β) of the polymer composite with varying conductive carbon compositions is measured and calculated using equation 1 [28], where ρ_a is the apparent density, and ρ_t is the actual density:

$$\beta = \left(\frac{1 - \rho_a}{\rho_t} \right) \times 100\% \quad (1)$$

In this study, apparent density refers to the ratio between the total mass and the volume of the polymer composite calculated using equation 2. Meanwhile, ρ_t representing the material's mass per real unit volume, essentially the volume of the material without any pores. In this research, its value depends on the mass and density of the conductive carbon used, calculated using equation 3 [29]:

$$\rho_a = \frac{m_{composite}}{V_{matrix} + V_{carbon}} \quad (2)$$

$$\rho_t = \frac{m_{composite}}{m_{carbon} \times \rho_{carbon}^{-1} + m_{CGG} \times \rho_{CGG}^{-1}} \quad (3)$$

Figure 3 illustrates the values of apparent density and porosity for each polymer composite sample. The apparent density of the CGG sample is 1.77 g/cm³, and when CNT is introduced into the polymer composite, the apparent density increases to 2 g/cm³. The addition of graphite or carbon foam also results in a change in the apparent density (ρ_a), and the formed trend shows an overall increase. The ρ_t value for the CGG sample is 6.52 g/cm³, then decreases significantly when CNT is incorporated. Other conductive carbons, namely graphite and carbon foam, also form polymer composite materials with a tendency to gradually increase the ρ_t value.

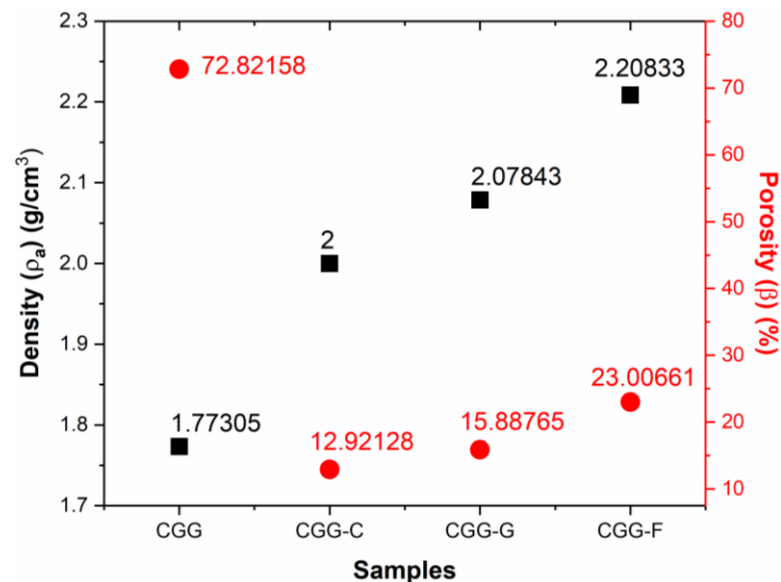


Figure 3. Density and porosity of CGG, CGG-C, CGG-G, and CGG-F samples

The ρ_a value for the CGG-C sample becomes the lowest because the density of CNT is relatively smaller compared to the density of graphite or carbon foam. Porosity exhibits an inverse relationship with apparent density; the lower the porosity value, the higher the apparent density of the sample. Importantly, the inverse relationship between porosity and apparent density suggests that the incorporation of conductive carbons contributes to reducing the polymer composite's mass density. The apparent density and porosity values presented in Figure 3 offer valuable insights into the effects of different conductive carbon compositions on the polymer composite samples [30]. This low-density characteristic holds promise, particularly for applications in electronic devices like batteries and fuel cells [31].

3.3. Scanning Electron Microscope (SEM)

Figure 4 shows SEM images of the surface of the CGG sample at magnifications of 500 and 1000 times. The mixture of corn starch with natural rubber produces a dense and clumpy surface for the polymer composite. Using ImageJ application, the particle grain size of the sample is determined to be 2-3 μm , consistent with the findings of a study by [21]. The sample surface appears as clusters without distinct grain boundaries, attributed to the aggregative nature of both corn starch and natural rubber. This characteristic implies a tendency for particle adhesion between particles of similar and different types. Additionally, CMC is used as a crosslinking agent in the polymerization process of the sample. While the addition of this agent does not alter the particle size, it can strengthen the interactions between natural rubber and corn starch particles.

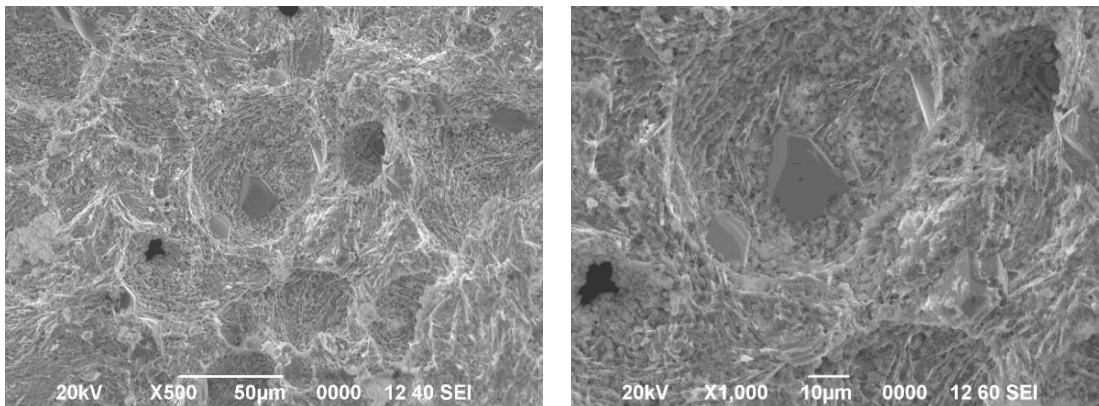


Figure 4. SEM image of CGG sample

Figure 5 displays SEM images of the surface morphology of the CGG-C sample at magnifications of 500 and 1000 times. Based on measurements using the ImageJ application, the particle grain size of the sample is determined to be 1-1.5 μm . This result contrasts with the sample without the addition of CNT into the CGG polymer composite, where the grain size decreases when 0.6 grams of CNT are present. This phenomenon can be attributed to the uniform dispersion nature of CNT, leading to the separation of grains, as evidenced in the SEM images [32]. The particle shape appears as plates or flakes randomly scattered across the entire surface of the sample.

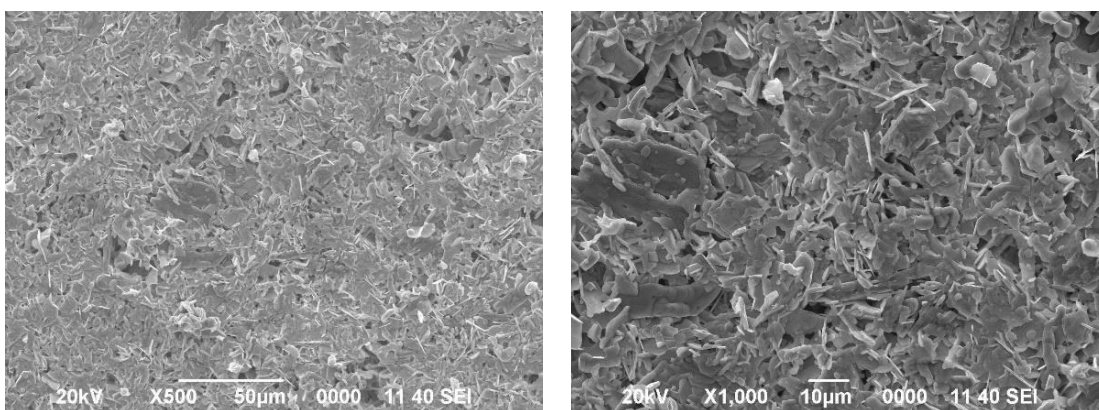


Figure 5. SEM image of CGG-C sample

Figure 6 shows SEM images of the surface morphology of the CGG-G sample at magnifications of 500 and 1000 times. It is evident that the sample undergoes a change in the distribution of grain sizes, appearing more uniform compared to the sample without the addition of graphite. This indicates that each particle of natural rubber and corn starch is uniformly dispersed due to the influence of interaction with graphite. The particle grain size of the sample ranges from 0.1 to 1.5 μm with a relatively high density. Graphite also exhibits an aggregative nature, enhancing adhesion with other particle types, including non-conductive polymers like corn starch. At 1000 times magnification, clear boundaries between grains are visible, indicating an increase in the active surface area. This condition can facilitate the electron transfer process within the formed conductive pathway [33].

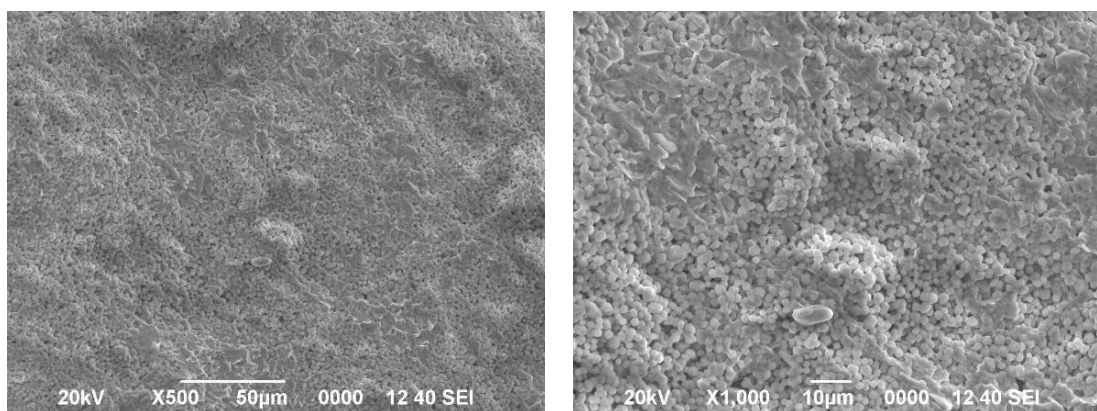


Figure 6. SEM image of CGG-G sample

Figure 7 presents SEM morphology images of the CGG-F sample at magnifications of 500 and 1000 times. The addition of the conductive carbon type, carbon foam, into the CGG polymer composite results in a surface morphology with granular shapes resembling porous tubes with high density. The measured particle grain size through ImageJ is determined to be 0.1-1.5 μm , similar to the CGG-G sample. The image at 1000 times magnification reveals the formation of fibers between the homogenous composite matrix and porous grains. The reduced particle size and high porosity contribute to a high specific surface area, enabling an increased flow of electrons within the conductive pathway of the CGG polymer composite.

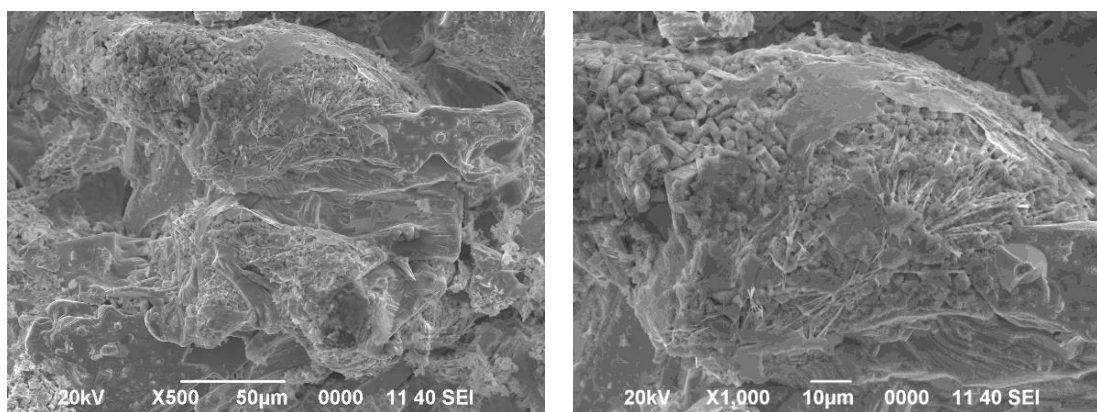


Figure 7. SEM image of CGG-F sample

3.4. Electrical Conductivity

Figure 8 illustrates the curve depicting the relationship between electrical conductivity values and frequency function for all samples. It can be observed that the electrical conductivity values of the CGG sample range from 10^{-7} to $3.75 \times 10^{-7} \text{ S.cm}^{-1}$ and increase to the range of 6×10^{-4} to $1.4 \times 10^{-3} \text{ S.cm}^{-1}$ for the CGG-C sample. This indicates that the addition of 6% CNT by the total mass of the CGG polymer composite supports the development of its electrical conductivity properties inside composite polymer structure [34,35].

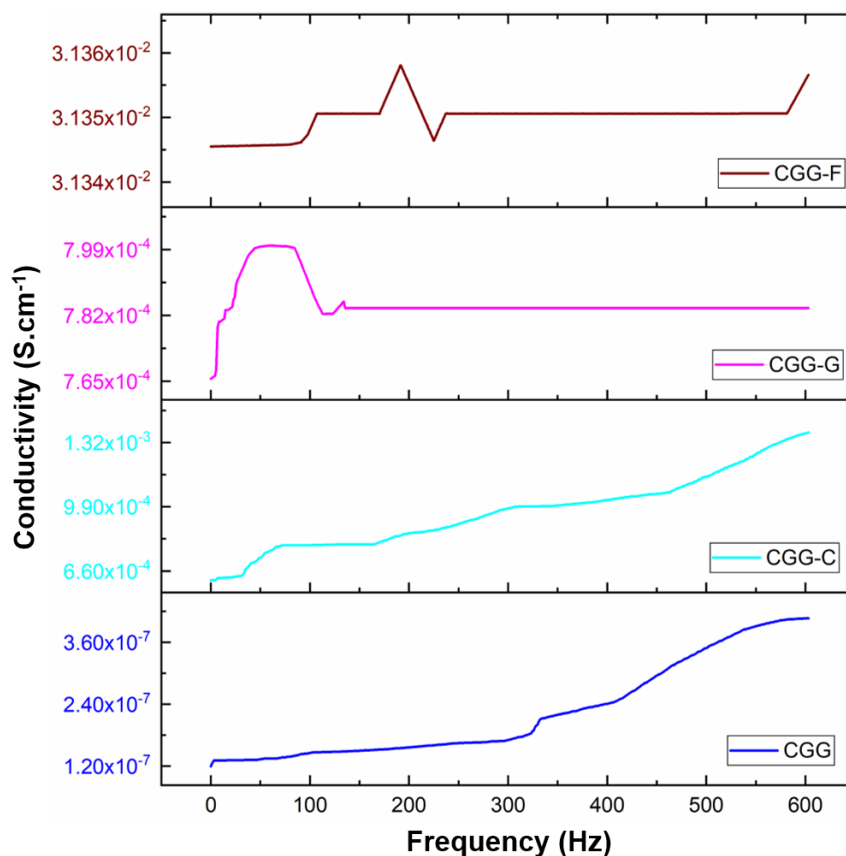


Figure 8. Curve of electrical conductivity versus frequency function for samples CGG, CGG-C, CGG-G and CGG-F

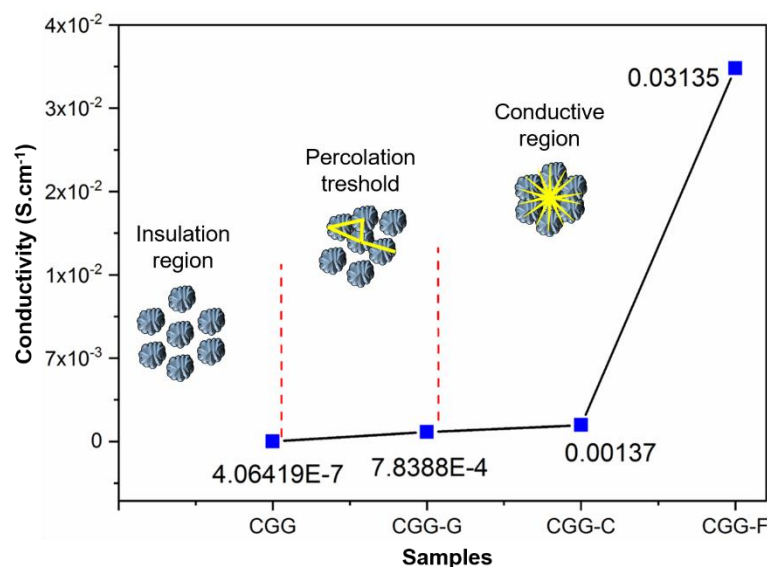
The presence of CNT particles in the composite matrix forms conductivity pathways within its structure, allowing electrons to flow from positive to negative poles. Table 2 presents the electrical conductivity values of CNT, graphite, and carbon foam, where CNT exhibits an electrical conductivity of $3.8 \times 10^5 \text{ S.cm}^{-1}$. While this value can support high electron transitions, since 84% of the CGG-C conductive polymer composite is a polymer matrix, the resulting electrical conductivity does not reach the same level as CNT. However, increasing the mass of CNT might lead to enhanced conductivity [36], though mechanical resistance may be affected due to a potential reduction in the polymer's elasticity with increased CNT substitution in its structure. Furthermore, the increased conductivity values concerning frequency function in the CGG-C sample indicate the instability of the CNT conduction pathway in the CGG polymer composite. This observation suggests that, as the frequency rises, the conductivity pathway involving CNT experiences variations, possibly due to disruptions or reconfigurations in the conductive network [32].

Table 2. Comparison of electrical conductivity values (σ) of samples

Carbons	σ (S.cm ⁻¹) [10]	Polymer composites	σ at freq. 600 Hz (S.cm ⁻¹) (this study)
CNT	3,8x10 ⁵	CGG-C	1.369 x 10 ⁻³
Graphite	10 ⁴	CGG-G	7.838 x 10 ⁻⁴
Carbon foam	10 ⁵	CGG-F	3,135 x 10 ⁻²

The electrical conductivity curve of the CGG-G sample indicates values ranging from 7.65×10^{-4} to 7.99×10^{-4} S.cm⁻¹ within the frequency range of 0-100 Hz. These values are nearly identical to those of the CGG-C sample within the same frequency range but then decrease until the frequency reaches 150 Hz. Further frequency increases do not lead to an increase or decrease in electrical conductivity values, indicating that within the 150-600 Hz range, the graphite conduction pathway in the CGG polymer composite has reached stability. However, when compared to the CGG-C sample, the average electrical conductivity value of the CGG-G sample is still lower by a difference of 6.15×10^{-4} S.cm⁻¹. This condition likely results from the surface morphology formed on the CGG-C sample, which has a plate-like (flat) structure with lower density compared to the grain density in the CGG-G sample morphology.

The CGG-F sample exhibits a more stable conductivity curve compared to other samples. At a frequency of 0.1 Hz, the measured electrical conductivity value is 3.134×10^{-2} S.cm⁻¹. The curve line shows increases and decreases, but upon closer inspection, the increase from 0.1 Hz to 105.96 Hz only experiences a slight addition of electrical conductivity value by 3×10^{-6} S.cm⁻¹, and the decrease in electrical conductivity from the frequency of 191.72 Hz to 225.22 Hz is only 7.837×10^{-6} S.cm⁻¹. Above 300 Hz, the CGG-F sample demonstrates stability in electrical conductivity values. Dominantly, the conduction pathway in this sample has a stable conductivity structure. Figure 9 illustrates the conductivity conditions of each polymer composite sample. It can be seen that the CGG sample at a frequency of 600 Hz has an electrical conductivity value of 4.064×10^{-7} S.cm⁻¹, which represents insulation or isolation conditions. This indicates a segregated or separated region among composite matrix particles due to the absence of pathways that electrons can traverse when flowing within it.

**Figure 9.** Illustration of the electrical conductivity properties of the sample

The CGG sample, based on non-conductive polysaccharides, lacks conductive pathways supporting electron transfer processes among particles. The addition of 0.6 grams of graphite to 10 grams of CGG is capable of forming several networks of conductive pathways in the composite, reaching the percolation threshold, which is the condition that has reached the initial limit of conductive pathway formation among some particles. CGG-C and CGG-F samples have dominantly formed perfect conductive pathway structures, allowing for comprehensive electron transfer processes within the polymer composite structure [37].

4. Conclusion

The incorporation of conductive carbons, including CNT, graphite, and carbon foam, into polymer composites resulted in a reduction in density. Notably, samples containing carbon foam demonstrated optimal porosity compared to other carbon variants. The surface morphology of CGG-C exhibited stacked plate-like structures with lower density, while CGG-F displayed a tubular porous morphology with relatively higher density. Furthermore, the addition of CNT, graphite, and carbon foam established conductive pathways within the corn starch-based polymer composites. At a frequency of 0.1 Hz, electrical conductivity values for samples without carbon, CNT-added, graphite-added, and carbon foam-added were measured at 1.192×10^{-7} , 6.123×10^{-4} , 7.656×10^{-4} , and 3.134×10^{-2} S.cm⁻¹, respectively. Notably, the graphite-added composite achieved a relatively higher electrical conductivity of 7.838×10^{-4} S.cm⁻¹.

References

- [1] Idumah C I. (2021). Novel trends in conductive polymeric nanocomposites, and bionanocomposites. *Synthetic Metals*, 273 116674.
- [2] Peng S, Yu Y, Wu S and Wang C-H. (2021). Conductive Polymer Nanocomposites for Stretchable Electronics: Material Selection, Design, and Applications. *ACS Applied Materials & Interfaces*, 13 43831–54.
- [3] Rashid A Bin and Hoque M E. (2022). Polymer nanocomposites for defense applications. *Advanced Polymer Nanocomposites* (Elsevier) pp 373–414
- [4] Biglari N and Zare E N. (2024). Conjugated polymer-based composite scaffolds for tissue engineering and regenerative medicine. *Alexandria Engineering Journal*, 87 277–99.
- [5] Kanoun O, Bouhamed A, Ramalingame R, Bautista-Quijano J R, Rajendran D and Al-Hamry A. (2021). Review on Conductive Polymer/CNTs Nanocomposites Based Flexible and Stretchable Strain and Pressure Sensors. *Sensors*, 21 1–29.
- [6] Schmitz D P, Santana L, Barra G M O and Soares B G. (2024). 3D printed honeycomb bilayer structures based on polylactic acid as lightweight microwave absorbing materials. *Polymers for Advanced Technologies*, 35
- [7] Zheng S, Wang Y, Zhu Y and Zheng C. (2024). Recent advances in structural design of conductive polymer composites for electromagnetic interference shielding. *Polymer Composites*, 45 43–76.
- [8] Zhou Y, Burgoyne Morris G H and Nair M. (2024). Current and emerging strategies for biocompatible materials for implantable electronics. *Cell Reports Physical Science*, 101852.
- [9] Estanto E, Bonardo D, Suyatman S and Nuruddin A. (2024). The Influence of 2-Methoxyethanol as Capping Agent on WO₃-Based Carbon Monoxide Gas Sensor Characteristics. *Journal of Physics: Conference Series*, 2705 012017.
- [10] Huang Y, Kormakov S, He X, Gao X, Zheng X, Liu Y, Sun J and Wu D. (2019). Conductive Polymer Composites from Renewable Resources: An Overview of Preparation, Properties, and Applications. *Polymers*, 11
- [11] Sharma S, Sudhakara P, Omran A A B, Singh J and Ilyas R A. (2021). Recent Trends and Developments in Conducting Polymer Nanocomposites for Multifunctional Applications.

- Polymers*, 13 2898.
- [12] Lux F. (1993). Models proposed to explain the electrical conductivity of mixtures made of conductive and insulating materials. *Journal of Materials Science*, 28 285–301.
- [13] Xu H, Cheng H, McClements D J, Chen L, Long J and Jin Z. (2022). Enhancing the physicochemical properties and functional performance of starch-based films using inorganic carbon materials: A review. *Carbohydrate Polymers*, 295 119743.
- [14] Dua S, Arora N, B. G. P, Saxena R C, Ganguly S K and T. S. (2024). Conjugated polymer-based composites for anti-corrosion applications. *Progress in Organic Coatings*, 188 108231.
- [15] Wang Y and Feng W. (2022). Introduction of Conductive Polymers. *Conductive Polymers and Their Composites* (Singapore: Springer Nature Singapore) pp 1–31
- [16] Sumdani M G, Islam M R, Yahaya A N A and Safie S I. (2022). Recent advancements in synthesis, properties, and applications of conductive polymers for electrochemical energy storage devices: A review. *Polymer Engineering & Science*, 62 269–303.
- [17] Amin M R, Chowdhury M A and Kowser M A. (2019). Characterization and performance analysis of composite bioplastics synthesized using titanium dioxide nanoparticles with corn starch. *Heliyon*, 5
- [18] Yemata T A, Ye Q, Zhou H, Kyaw A K K, Chin W S and Xu J. (2017). *Conducting polymer-based thermoelectric composites: Principles, processing, and applications* (Elsevier Ltd)
- [19] Wu Y, Wang Z, Liu X, Shen X, Zheng Q, Xue Q and Kim J K. (2017). Ultralight Graphene Foam/Conductive Polymer Composites for Exceptional Electromagnetic Interference Shielding. *ACS Applied Materials and Interfaces*, 9 9059–69.
- [20] Chatterjee S, Mahmood S, Hilles A R, Thomas S, Roy S, Provaznik V, Romero E L and Ghosal K. (2023). Cationic starch: A functionalized polysaccharide based polymer for advancement of drug delivery and health care system - A review. *International Journal of Biological Macromolecules*, 248 125757.
- [21] Leksawasdi N, Chaiyaso T, Rachtanapun P, Thanakkasaranee S, Jantrawut P, Ruksiriwanich W, Seesuriyachan P, Phimolsiripol Y, Techapun C, Sommano S R, Ougizawa T and Jantanasakulwong K. (2021). Corn starch reactive blending with latex from natural rubber using Na⁺ ions augmented carboxymethyl cellulose as a crosslinking agent. *Scientific Reports*, 11 1–10.
- [22] Kwon Y-J, Park J-B, Jeon Y-P, Hong J-Y, Park H-S and Lee J-U. (2021). A Review of Polymer Composites Based on Carbon Fillers for Thermal Management Applications: Design, Preparation, and Properties. *Polymers*, 13 1312.
- [23] B.A P, N L, Buradi A, N S, B L P and R V. (2022). A comprehensive review of emerging additive manufacturing (3D printing technology): Methods, materials, applications, challenges, trends and future potential. *Materials Today: Proceedings*, 52 1309–13.
- [24] Bonardo D, Septiani N L W, Estananto E, Suyatman S, Humaidi S and Yulianto B. (2023). Synthesis and characterization of WO₃ sensitive layers for NO₂ gas sensor application. p 050012
- [25] Agrawal P R, Kumar R, Teotia S, Kumari S, Mondal D P and Dhakate S R. (2019). Lightweight, high electrical and thermal conducting carbon-rGO composites foam for superior electromagnetic interference shielding. *Composites Part B: Engineering*, 160 131–9.
- [26] Petit T and Puskar L. (2018). FTIR spectroscopy of nanodiamonds: Methods and interpretation. *Diamond and Related Materials*, 89 52–66.
- [27] Estananto E, Utari L, Septiani N L W, Bonardo D, Nuruddin A, Suyatman S and Yulianto B. (2023). Anatase TiO₂ on graphene-coated cotton flexible sensor at room temperature. p 050032

-
- [28] Zhang D, Liu L, Lan X, Li F, Liu Y and Leng J. (2023). Experimental study on nonlinearity of unidirectional carbon fibre-reinforced shape memory polymer composites. *Composites Part A: Applied Science and Manufacturing*, 166 107372.
- [29] Najmi L and Hu Z. (2023). Effects of Carbon Nanotubes on Thermal Behavior of Epoxy Resin Composites. *Journal of Composites Science*, 7 313.
- [30] Bonardo D, Septiani N L W, Amri F, Estanto, Humaidi S, Suyatman and Yulianto B. (2021). Review—Recent Development of WO₃ for Toxic Gas Sensors Applications . *Journal of The Electrochemical Society*, 168 107502.
- [31] Tadesse M G, Ahmmed A S and Lübben J F. (2024). Review on Conductive Polymer Composites for Supercapacitor Applications. *Journal of Composites Science*, 8 53.
- [32] Wang M, Tang X H, Cai J H, Wu H, Shen J Bin and Guo S Y. (2021). Construction, mechanism and prospective of conductive polymer composites with multiple interfaces for electromagnetic interference shielding: A review. *Carbon*, 177 377–402.
- [33] Bonardo D, Darsono N, Humaidi S, Imaduddin A and Silalahi N S. (2023). Effect of calcination frequency on the thermoelectric properties of Ti doped CuCrO₂ by solid state method. *Journal of Metals, Materials and Minerals*, 33 1785.
- [34] Vandghanooni S and Eskandani M. (2019). Electrically conductive biomaterials based on natural polysaccharides: Challenges and applications in tissue engineering. *International Journal of Biological Macromolecules*, 141 636–62.
- [35] Wang Y and Weng G J. (2018). Electrical Conductivity of Carbon Nanotube- and Graphene-Based Nanocomposites. *Micromechanics and Nanomechanics of Composite Solids* (Cham: Springer International Publishing) pp 123–56
- [36] Kondrashov S V., Soldatov M A, Gunyaeva A G, Shashkeev K A, Komarova O A, Barinov D Y, Yurkov G Y, Shevchenko V G and Muzafarov A M. (2018). The use of noncovalently modified carbon nanotubes for preparation of hybrid polymeric composite materials with electrically conductive and lightning resistant properties. *Journal of Applied Polymer Science*, 135 2–9.
- [37] Peidayesh H, Mosnáčková K, Špitalský Z, Heydari A, Šišková A O and Chodák I. (2021). Thermoplastic starch-based composite reinforced by conductive filler networks: Physical properties and electrical conductivity changes during cyclic deformation. *Polymers*, 13